Capacity Optimization of Renewable Energy Sources and Battery Storage in an Autonomous Telecommunication Facility

Dragicevic, Tomislav; Pandži, Hrvoje; Škrlec, Davor; Kuzle, Igor; Guerrero, Josep M.; Kirschen, Daniel

Published in:
I E E E Transactions on Sustainable Energy

DOI (link to publication from Publisher):
10.1109/TSTE.2014.2316480

Publication date:
2014

Document Version
Accepted author manuscript, peer reviewed version

Capacity Optimization of Renewable Energy Sources and Battery Storage in an Autonomous Telecommunication Facility

Tomislav Dragičević, *Student Member, IEEE*, Hrvoje Pandžić, *Member, IEEE*, Davor Škrlec, *Member, IEEE*, Igor Kuzle, *Senior Member, IEEE*, Josep M. Guerrero, *Senior Member, IEEE*, and Daniel S. Kirschen, *Fellow, IEEE*

***Abstract*—This paper describes a robust optimization approach to minimize the total cost of supplying a remote telecommunication station exclusively by renewable energy sources (RES). Due to intermittent nature of RES, such as photovoltaic (PV) panels and small wind turbines, they are normally supported by a central energy storage system (ESS), consisting of a battery and a fuel cell. The optimization is carried out as a robust mixed-integer linear program (RMILP), and results in different optimal solutions, depending on budgets of uncertainty, each of which yields different RES and storage capacities. These solutions are then tested against a set of possible outcomes, thus simulating the future operation of the system. Since battery cycling is inevitable in this application, an algorithm that counts the number of cycles and associated depths of discharges (DoD) is applied to the optimization results. The annual capacity reduction that results from these cycles is calculated for two types of battery technologies, i.e. valve-regulated lead-acid (VRLA) and lithium-ion (Li-Ion), and treated as an additional cost. Finally, all associated costs are added up and the ideal configuration is proposed.**

***Index Terms*—Autonomous power facility, batteries, energy storage system, renewable energy sources, robust mixed-integer linear programming.**

NOMENCLATURE

Parameters

$D\left(t\right)$	system demand (kW),
$H^{\max}$	hydrogen storage capacity (l),
$G_{\mathrm{bat}}^{\mathrm{ch,max}}$	maximum battery charging rate (kW),
$G_{\mathrm{bat}}^{\mathrm{dis,max}}$	maximum battery discharging rate (kW),
H^{cost}	hydrogen storage replacement cost (€),
K_{bat}	battery capacity specific cost (€/kWh),
K_{fc}	fuel cell specific cost (€/kW),
K_{hyd}	hydrogen to electricity conversion ratio (l/kW),
K_{pv}	photovoltaic panel specific cost (€/kW),
K_{w}	wind turbine specific cost (€/kW),
$PV^{\max}\left(t\right)$	normalized maximum PV output (kW/kW),
$S^{\min}$	minimum allowed SoC (%),
$W^{\max}\left(t\right)$	normalized maximum wind turbine output (kW/kW),
η_{ch}	charging efficiency of the battery,
η_{dis}	discharging efficiency of the battery.

Variables

c_{bat}	total battery storage capacity (kWh),
c_{fc}	fuel cell installed capacity (kW),
c_{pv}	photovoltaic panel installed capacity (kW),
c_{w}	wind turbine installed capacity (kW),
$g_{\mathrm{bat}}^{\mathrm{ch}}\left(t\right)$	electricity charged to the battery (kW),
$g_{\mathrm{bat}}^{\mathrm{dis}}\left(t\right)$	electricity discharged form the battery (kW),
$g_{\mathrm{fc}}\left(t\right)$	fuel cell generation (kW),
$g_{\mathrm{pv}}\left(t\right)$	PV generation (kW),
$g_{\mathrm{w}}\left(t\right)$	wind turbine generation (kW),
$l\left(t\right)$	curtailed RES output,
n_{hyd}	number of hydrogen storage replacements,
$s\left(t\right)$	battery state-of-charge (kWh),
$v_{\mathrm{fc}}\left(t\right)$	consumed hydrogen (l),
$x_{\mathrm{bat}}^{\mathrm{ch}}\left(t\right)$	binary variable equal to 1 if battery is being charged at time period t, and 0 otherwise,
$x_{\mathrm{bat}}^{\mathrm{dis}}\left(t\right)$	binary variable equal to 1 if battery is being discharged at time period t, and 0 otherwise.

I. INTRODUCTION

ELECTRICITY consumption of remote facilities, such as telecommunication stations, data centers or secluded households, is often too low to justify the investments required to connect them to a bulk power distribution network. In the past, electrical power supply of such systems was resolved using a single generating plant, typically a diesel generator set [1]. However, environmental concerns and the rising cost of fossil fuels have recently made renewable energy sources (RES), such as photovoltaic (PV) and wind, an attractive alternative [2], [3]. This trend has been further underpinned by rapid improvements in power electronics, which enabled full controllability of RES, within the constraints imposed by the natural phenomenon [4]. For isolated systems, due to the variable production of RES, it is common practice to combine them with some kind of an energy storage system (ESS), leading to the concept of microgrid [5], [6], [7], [8].

Over the past decade, intensive research efforts have been focused on improving real-time performance in both AC and DC coupled microgrid systems. These include targeting islanded control [9], energy management [10], stability enhancement [11], etc. More recently, methods such as intelligent control of power quality [12], [13], accurate power sharing between paralleled units [14], distributed secondary control [15], plug and play feature [16] and adaptive droop control [17]

have been proposed. Consequently, microgrids have reached a higher technological maturity and have become a suitable option for industrial applications. More than 3,793 MW of capacity has been installed in microgrids across the globe according to a recent report [18].

The key to achieving optimal long-term performance in an actual deployment lies in the planning and design stages of the project. At these stages, it is essential to properly estimate the uncertainty and volatility of RES and identify the way of dealing with those, e.g. by adding an ESS. The principal role of the ESS is to compensate for the long- and short-term imbalances between power generation and demand. The ESS is thus used to transfer energy from periods of high RES output to periods of power shortage, allowing the system to remain fully functional over a wide range of operating conditions. Additionally, a controllable power source may be used as a last resort. The most common choice is a diesel generator. However, in order to keep the system environmentally friendly, fuel cells may be considered. Since different power sources and technologies are involved, a fundamental question arises: What is the optimal RES generation and storage mix that guarantees the supply at minimum cost? The selection of the optimal RES mix, as well as the ESS capacity should be done with respect to initial installation and cumulative operating cost. Also, the solution needs to be validated to ensure that the required level of reliability of supply is achieved.

A number of papers dealing with the issue of designing small autonomous power systems are available. A comprehensive review of previous approaches to the problem may be found in [19]. These authors point out several popular commercial software packages, such as HOMER (Hybrid Optimization Model for Electric Renewable) and Hybrid2. They also briefly explain the applicability of other optimization routines, including the graphic construction method, the probabilistic approach, iterative techniques and artificial intelligence methods. Recent publications which were not covered by this review describe the calculation of the optimal capacity of pumped hydro storage with known wind turbine ratings and a diesel generator [20], a stochastic approach to a similar problem, but for a general ESS [21], studies on wind battery hybrid systems [22], [23], a simulated annealing algorithm [24] and a biogeography-based optimization algorithm [25]. However, none of these techniques takes advantage of the features of robust optimization nor considers the gradual loss of battery capacity over its lifespan. Moreover, full design flexibility was seldom addressed as the majority of these papers considers only the problem of sizing an EES when the capacities of the other components are taken as given.

The sources of uncertainty (load and RES generation) should be appropriately addressed in the optimization procedure. The most common way of dealing with uncertainty is stochastic optimization [26], which assumes that the probability distribution of uncertainty is known. Stochastic programming provides only a probabilistic guarantee of the quality of the solution. In practice, it is difficult to quantify accurately the probability distribution of the uncertainty. Furthermore, a large number of scenarios is required to obtain a solution with a high degree of significance [27]. This large number of scenarios results in a tremendous computational burden. In addition, the available historical data are often insufficient to generate a number of unbiased scenarios.

On the other hand, the robust optimization framework requires less detailed information regarding the uncertainty [28], which is described using only the range, i.e. upper and lower uncertainty bounds, rather than a set of scenarios. Furthermore, robust optimization incorporates a tuning parameter (the budget of uncertainty) that is used to adjust the robustness of the solution. Since the different values of the uncertainty budget yield more or less robust solutions, a Monte Carlo (MC) simulation is needed to find the optimal budget of uncertainty.

The cost of batteries typically plays a key role in the installation cost of small autonomous systems [29]. Therefore, their lifetime may have significant implications on total operational costs over the long-term, and should not be neglected. In particular, each charge/discharge cycle causes incremental reduction of usable battery capacity [30], [31]. It is generally accepted that once a battery capacity reduces by a certain percentage, the battery should be replaced as the nominal reliability cannot be guaranteed any more.

A rainflow counting algorithm is used to count the number of cycles over the time horizon. This algorithm is commonly used for fatigue analysis in structural engineering, power electronic systems and mechanical vibration applications [32], [33]. In this case, the rainflow counting method considers the state-of-charge (SoC) data as an input and calculates the equivalent cycles. The calculated capacity losses are converted into an additional cost, which is added to the objective function to identify the optimal battery technology.

This paper proposes an approach to determine the optimal power supply mix of an autonomous power system, while considering the detrimental impact of cycling on battery capacity. The optimization problem is formulated as a robust mixed-integer linear program (RMILP) that minimizes the total investment costs. The operation of the autonomous facility is simulated in order to identify the cheapest investment solution that satisfies the reliability requirements. For that purpose, a number of consumption/generation scenarios are generated based on measurements from an actual remote telecommunication facility. RES outputs are normalized to the actual output (kW) per installed capacity (kW), since RES capacities are decision variables.

The paper is organized as follows. Section II presents a deterministic formulation of the problem and expands it into a robust model. Section III gives the details of the combined cycling and depth-of-discharge (DoD) assessment algorithm based on the rain-flow counting method. In addition, the influence of these parameters on the incremental capacity reduction of the two most popular battery types, valve-regulated lead-acid (VRLA) and lithium-ion (Li-Ion), is investigated analytically. Section IV explains the solution algorithm. Section V presents the results of a case study. The conclusions of the paper and future research directions are provided in Section VI.

II. Problem Formulation

A. Deterministic Model

The deterministic problem is a mixed-integer linear problem formulated as follows:

Minimize

$$c_{\mathrm{pv}} \cdot K_{\mathrm{pv}} + c_{\mathrm{w}} \cdot K_{\mathrm{w}} + c_{\mathrm{bat}} \cdot K_{\mathrm{bat}} + c_{\mathrm{fc}} \cdot K_{\mathrm{fc}} + H^{\mathrm{cost}} \cdot n_{\mathrm{hyd}} \quad (1)$$

subject to

$$g_{\mathrm{pv}}(t) + g_{\mathrm{w}}(t) + g_{\mathrm{bat}}^{\mathrm{dis}}(t) \cdot \eta_{\mathrm{dis}} + g_{\mathrm{fc}}(t) = = D(t) + \frac{g_{\mathrm{bat}}^{\mathrm{ch}}(t)}{\eta_{\mathrm{ch}}} + l(t) \quad \forall t \in T \quad (2)$$

$$g_{\mathrm{pv}}(t) \leq PV^{\max}(t) \cdot c_{\mathrm{pv}} \quad \forall t \in T \quad (3)$$

$$g_{\mathrm{w}}(t) \leq W^{\max}(t) \cdot c_{\mathrm{w}} \quad \forall t \in T \quad (4)$$

$$g_{\mathrm{bat}}^{\mathrm{ch}}(t) \leq x_{\mathrm{bat}}^{\mathrm{ch}}(t) \cdot G_{\mathrm{bat}}^{\mathrm{ch,max}} \quad \forall t \in T \quad (5)$$

$$g_{\mathrm{bat}}^{\mathrm{dis}}(t) \leq x_{\mathrm{bat}}^{\mathrm{dis}}(t) \cdot G_{\mathrm{bat}}^{\mathrm{dis,max}} \quad \forall t \in T \quad (6)$$

$$x_{\mathrm{bat}}^{\mathrm{ch}}(t) + x_{\mathrm{bat}}^{\mathrm{dis}}(t) \leq 1 \quad \forall t \in T \quad (7)$$

$$s(t) = s(t-1) + g_{\mathrm{bat}}^{\mathrm{ch}}(t) - g_{\mathrm{bat}}^{\mathrm{dis}}(t) \quad \forall t \in T \quad (8)$$

$$S^{\min} \cdot c_{\mathrm{bat}} \leq s(t) \leq c_{\mathrm{bat}} \quad \forall t \in T \quad (9)$$

$$g_{\mathrm{fc}}(t) = \frac{v_{\mathrm{fc}}(t)}{K_{\mathrm{hyd}}} \quad \forall t \in T \quad (10)$$

$$\sum_{t=1}^{T} v_{\mathrm{fc}}(t) \leq H^{\max} \cdot n_{\mathrm{hyd}} \quad (11)$$

$$g_{\mathrm{fc}}(t) \leq c_{\mathrm{fc}} \quad \forall t \in T \quad (12)$$

The objective function (1) minimizes the overall investment cost, which includes the PV and wind capacity, total battery capacity, and the cost of installed fuel cells (including the hydrogen replacement cost). Equations (2) are power balance constraints for each time period. The left-hand side of this equality represents the net generation, while the right-hand side represents the net load. If the batteries are fully charged, some RES output might be curtailed, which is represented by the non-negative slack variable $l(t)$. The PV and wind turbine maximum outputs are defined by (3) and (4), respectively. The battery charging and discharging limits for each time period are imposed by constraints (5) and (6), respectively. Equations (7) ensure that the batteries cannot be charged and discharged at the same time. Equations (8) calculate the battery SoC, while the lower and upper limits on this SoC are imposed by (9). Constraints (10) are hydrogen volume-to-electricity conversion factors. The number of hydrogen replacements is calculated in (11). Finally, equations (12) enforce the limits on electricity generation by the fuel cell.

B. Robust Model

The formulation (1)-(12) is valid only if all parameters are deterministic. However, the specific PV output $PV^{\max}(t)$, the specific wind turbine output $W^{\max}(t)$ and the system demand $D(t)$ are uncertain. In this paper their values are assumed to remain within the known boundaries.

In order to design a minimum investment cost system that is able to supply the load at all times, even during the periods of low RES output, a robust optimization approach is applied. The mathematical apparatus for robust optimization proposed in [28] provides full control of the degree of conservatism for each uncertain parameter. Robust optimization has already been applied to the optimization of offering strategies in electricity markets [34] and to the security-constrained unit commitment problem [35]. The most salient feature of this approach is that its solution is feasible even for the worst-case scenario, which makes it appropriate for defining the optimal RES generation mix and the optimal storage capacity at a remote telecommunication facility.

Problem (1)-(12) can be expressed in the following general form:

$$\text{Minimize} \quad \sum_{j=1}^{n} c_j x_j \quad (13)$$

subject to

$$\sum_{j=1}^{n} a_{ij} x_j \leq b_i \quad (14)$$

$$x_j \geq 0 \quad (15)$$

where some of the coefficients a_{ij} are uncertain. Uncertain coefficients have values within the interval $[a_{ij} - \hat{a}_{ij}]$ where $\hat{a}_{ij}$ represents deviation from the nominal value of coefficient a_{ij}. A budget of uncertainty Γ_i is used to control the conservatism of the interval $[a_{ij} - \hat{a}_{ij}]$. Γ_i takes values over the interval $[0, |J|]$, where $J = \{j \mid \hat{a}_{ij} \geq 0\}$. If $\Gamma_i = 0$, no deviations from the nominal value of uncertain parameter are considered, which corresponds to the least conservative, and thus the least expensive solution. On the other hand, if $\Gamma_i = |J|$, a full deviation is considered, which corresponds to the most conservative and most expensive case.

As an example, let us consider a case where the wind output is expected to vary between 100 and 150 kW at a certain time period. This means that $a = 150$, $\hat{a} = 50$, $J = 1$. If Γ is equal to zero, the model will consider the wind output to be 150 kW, resulting in a risky solution because the actual wind output might be as low as 100 kW (assuming that the given interval is correct). On the other hand, if Γ is equal to 1, the most conservative case of only 100 kW wind output will be considered and the resulting solution will be protected against this low realization of wind output.

The robust counterpart of the original problem (13)-(15) is then:

$$\text{Minimize} \quad \sum_{j=1}^{n} c_j x_j \quad (16)$$

subject to

$$\sum_{j=1}^{n} a_{ij}x_j - z_i \cdot \Gamma_i - \sum_{j=1}^{n} p_{ij} \leq b_i \tag{17}$$

$$z_i + \sum_{j=1}^{n} p_{ij} \geq \hat{a}_{ij} \tag{18}$$

$$x_j \geq 0 \tag{19}$$

A detailed description of this procedure is available in [28].

In the deterministic model (1)-(12) all uncertain parameters appear in the power balance equation (2). Its robust form is:

$$\begin{aligned} g_{\mathrm{pv}}(t) - p_{\mathrm{pv}}(t) - z_{\mathrm{pv}} \cdot \Gamma_{\mathrm{pv}} + g_{\mathrm{w}}(t) - p_{\mathrm{w}}(t) - z_{\mathrm{w}} \cdot \Gamma_{\mathrm{w}} + \\ + g_{\mathrm{bat}}^{\mathrm{dis}}(t) \cdot \eta_{\mathrm{dis}} + g_{\mathrm{fc}}(t) = D(t) + p_{\mathrm{d}}(t) + z_{\mathrm{d}} \cdot \Gamma_{\mathrm{d}} + \\ + \frac{g_{\mathrm{bat}}^{\mathrm{ch}}(t)}{\eta_{\mathrm{ch}}} + l(t) \quad \forall t \in T \end{aligned} \tag{20}$$

Where $p_{\mathrm{pv}}(t)$ is the dual variable of constraint (3), while z_{pv} is used to obtain linear expressions. These non-negative variables are used to model the uncertainty of the PV output, which is controlled by the uncertainty budget Γ_{pv}, ranging from 0 (the most optimistic case), to 1 (the most pessimistic case). The corresponding non-negative auxiliary variables for the wind turbine output uncertainty are $p_{\mathrm{w}}(t)$, the dual variable of equation (4), and z_{w}, used to obtain linear expressions. The dual variable of equation (2), $p_{\mathrm{d}}(t)$, and the auxiliary variable z_{d}, used for linearization purposes, are used to model the demand uncertainty. In order to consider the uncertainty ranges, the following constraints need to be added:

$$z_{\mathrm{pv}} + p_{\mathrm{pv}}(t) \geq \left(PV^{\max}(t) - PV^{\min}(t)\right) \cdot c_{\mathrm{pv}} \quad \forall t \in T \tag{21}$$

$$z_{\mathrm{w}} + p_{\mathrm{w}}(t) \geq \left(W^{\max}(t) - W^{\min}(t)\right) \cdot c_{\mathrm{w}} \quad \forall t \in T \tag{22}$$

$$z_{\mathrm{d}} + p_{\mathrm{d}}(t) \geq \left(D^{\max}(t) - D^{\min}(t)\right) \cdot c_{\mathrm{d}} \quad \forall t \in T \tag{23}$$

Equations (21)-(23) force the auxiliary variables to take values greater or equal than the base uncertain values plus the uncertainty range. The distribution of values between them depends on the uncertainty budgets. For the PV output in (21), if Γ_{pv} is equal to 0, variable $p_{\mathrm{pv}}(t)$ will be equal to zero as the value of the uncertainty range will be assigned to z_{pv}. Since z_{pv} is multiplied by Γ_{pv} in (20), that is 0, equation 20 will be identical to (2). On the other hand, if Γ_{pv} is equal to one, both $p_{\mathrm{pv}}(t)$ and z_{pv} affect equation (20) forcing an increase in installed capacity. Similar considerations are valid for wind and demand uncertainty in constraints (22) and (23).

The final RMILP is formulated as follows:

$$(1)$$

subject to:

$$(3) - (12), \quad (20) - (23)$$

III. The Influence of Battery Degradation

In applications where reliability plays an important role, it is desirable to credibly estimate the health status of critical devices. The battery of an RES-based autonomous telecommunication facility is such a critical device. Since it is used to balance the load and the RES output, every deviation from the power equilibrium is reflected in its SoC, which therefore undergoes repeated charge/discharge cycles of various depths. The impact of each cycle and its respective DoD on the incremental reduction in battery capacity is well documented and has been extensively studied for different battery technologies [36]. A summary of cycling-based capacity deterioration for two popular battery technologies is given below, and is followed by an explanation of how this effect is modeled in this paper. It should be noted at this point that in objective function (1), the total, i.e. initial, battery capacity is determined. As time passes, the actual usable capacity decreases.

A. Impact of Cycling to a Battery Technology

Repeated deep cycling has an adverse effect on the battery lifetime because it results in a gradual reduction in available energy storage capacity. The deeper the discharge cycles are, the more of incremental capacity is lost. Experimental life-cycle tests are usually carried out by exposing the batteries to charge/discharge cycles with consistent DoD [37], [38]. The process is repeated until the usable battery capacity falls below a predetermined percentage of its initial value, which is considered to be the end of its life [39].

Then, after organizing the recorded data in N_{cycle} vs. DoD diagram, the incremental impact of one cycle of a specific depth may be computed as follows:

$$C_{loss}\left(\frac{\%}{cycle}\right) = \frac{20}{N_{cycle}(DoD)} \tag{24}$$

where C_{loss} is the percentage of capacity loss per cycle, while $N_{cycle}(DoD)$ is the number of cycles which leads to end of life when the battery is repeatedly cycled to a specific DoD. The characteristics of the two technologies that dominate the battery market today, i.e. VRLA and Li-Ion, are examined below.

1) VRLA: Due to attractive combination of low-price and relatively good performance, VRLA technology accounts for well over 70% of telecommunication batteries today [36]. However, this type of battery has several main disadvantages, namely a narrow temperature operating range and a short lifetime. Thus, even though the application of VRLA technology generally results in the lowest initial cost, its long-term economic viability should be addressed more rigorously. Fitting the data from [37] into an exponential function and combining it with (24), the incremental percentage of capacity loss per cycle for a typical VRLA battery may be expressed as follows:

$$C_{VRLA} = \frac{20}{6188 \cdot e^{-0.02769 \cdot DoD_{cyc}} + 13.81} \tag{25}$$

where DoD_{cyc} is the depth of cycle under consideration.

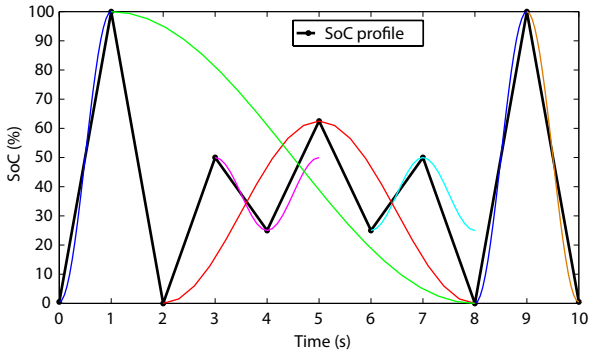

Fig. 1. Cycle extraction strategy applied to the exemplary SoC profile.

2) Li-Ion: The cycling wear-and-tear effect of this battery technology is much less pronounced than for VRLA because its electrochemical processes are fundamentally different. In particular, instead of changing the structure of the electrodes at every cycle, the charge/discharge process consists mostly of transferring lithium ions between the positive and the negative plates. Moreover, the specific energy (150 Wh/kg) and energy density (400 Wh/l) of Li-Ion batteries outperforms all other battery types [36]. Consequently, its share of the market has experienced a rapid growth over the past decade, despite considerable cost. Data for calculation of the incremental loss percentage per cycle for Li-Ion battery is taken from [40] and fitted into an exponential curve. Combined with (24), this yields the incremental percentage capacity loss per cycle for a typical Li-Ion battery:

$$C_{Li-Ion} = \frac{20}{33000 \cdot e^{-0.06576 \cdot DoD_{cyc}} + 3277} \qquad (26)$$

B. Cycle-Counting Algorithm

In order to calculate the total capacity loss over a given time horizon, equations (25) and (26) need to be evaluated for every cycle that occurs. Therefore, the total number of cycles and their respective DoDs must be computed. To that end, SoC data must be determined from the dispatch strategy suggested by the optimization algorithm. However, the SoC variable should be normalized to adopt values up to 100. Since the cycle numbering in the proposed method is performed after the optimization procedure, a classical off-line form of the rain-flow counting algorithm is applied [41]. This algorithm pairs local SoC minima and maxima and defines equivalent half and full cycles. Figure 1 shows an example of the cycle-counting mechanism applied to an arbitrarily generated SoC profile (bold black line). The algorithm detects three full cycles (red, magenta and light blue curves) and four-half cycles (blue, green, blue and orange curves). Pairs of up and down half-cycles are approximated as a full cycle. A detailed explanation of the application of the rain-flow counting algorithm is available in [41].

IV. Solution Algorithm

Figure 2 illustrates the overall solution procedure. The required input data are solar irradiation and wind speed

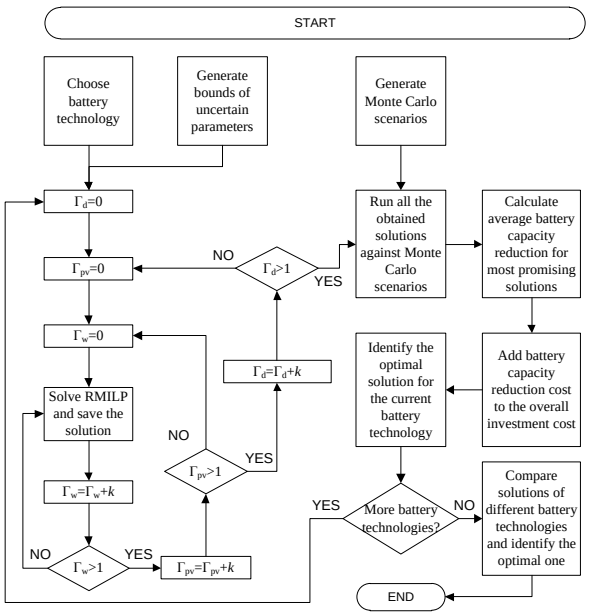

Fig. 2. Solution algorithm.

measurements that need to be converted to power output using the manufacturer data for the solar panel and the wind turbine. Since telecommunication equipment demand cannot be forecast, historical data of similar telecommunications facility is used. The step-by-step procedure is as follows:

1) Based on measurements and historical data define upper and lower bounds of uncertain parameters, i.e. wind power output, PV power output and demand.
2) Select the initial battery technology.
3) Set budgets of uncertainty for all three uncertain parameters to zero. This corresponds to the best case scenario, i.e., load equal to the lower bound, and RES outputs equal to their upper bounds at all time periods.
4) Apply the RMILP to calculate the solution for these values of the uncertainty parameters and save this solution.
5) Increase the uncertainty budget of wind power output in steps of k. Small value of parameter k, e.g., 0.01, will result in a fine resolution of solutions. However, the computing time required increases like the cube of the number of steps in k because this parameter is used for three uncertain values. On the other hand, large values of k, e.g., 0.5, will result in large gaps between the solutions and the final solution will be far away from the global optimum. Note that different values of k can be used for each uncertain parameter.
6) If the wind uncertainty budget is less or equal than one, go to step 4. Otherwise, increase the PV output uncertainty budget by k, reset the uncertainty budget for wind power output to zero, and go back to step 4.
7) When the PV uncertainty budget exceeds 1, increase the demand uncertainty budget by k. If the demand uncertainty budget did not exceed 1, reset the uncertainty budgets for wind and PV output to zero, and go back to

step 4.

8) Based on measurements and historical data generate a sufficient number of MC scenarios.
9) Run all the RMILP solutions against the MC scenarios.
10) Since the battery significantly degrades when its SoC is reduced below a certain value [39], identify solutions with the lowest battery SoC throughout the year being just above the threshold.
11) Calculate the average battery capacity reduction for the most promising solutions.
12) Add the cost of battery capacity reduction to the overall investment cost.
13) Identify and save the optimal solution for the current battery technology.
14) Choose another battery technology and go to step 3. If there are no more technologies to consider, compare the optimal solutions for each technology and choose the one with the minimum total cost. This is the global optimum.

Instead of imposing a hard constraint for the minimum SoC at step 10, one may decide to introduce a penalty function that would increase the overall cost of solutions that incur SoC below a predetermined threshold. This would increase the average battery capacity reduction at step 11 and would expand the suitable candidates for the optimal solution. However, deriving such penalty functions for different battery technologies is outside the scope of this paper.

V. Case Study

A. Input Data

The input data were measured at an actual remotely located telecommunications facility at 15-minute intervals over three years. Measured variables were PV an wind generation, and demand. In order to limit the number of variables and decrease the computational burden, an hourly averaging was performed. The comparison indicated that using 1-hour intervals underestimated the battery degradation by 2% compared to the results that would be obtained with a 15-minute resolution. This is because at a finer time resolution the depth of the captured cycles becomes smaller. Since the incremental capacity loss over one cycle depends on its depth, the net impact of shallow cycles is much smaller than the impact of deep cycles. The effect of the cycles that were not captured because of this simplification was shown to be insignificant.

The lower and upper bounds of three uncertain parameters at each hour of the year are set to the minimum and maximum of the measured values. The RES output values are scaled to 1 kW of installed capacity. The average capacity utilization factors of the wind and PV generations are 21.4% and 19.1%. In Figure 3, the RES output values are scaled to 1 kW of installed capacity, while the demand curve shows actual values. For a small number of days, the maximum demand exceeds 1 kW. The demand uncertainty range is almost constantly around 300 W. The wind generation duration curve has a similar shape, with higher uncertainty ranges at higher power outputs. The maximum PV output curve is much steeper because the PV output is zero during the night.

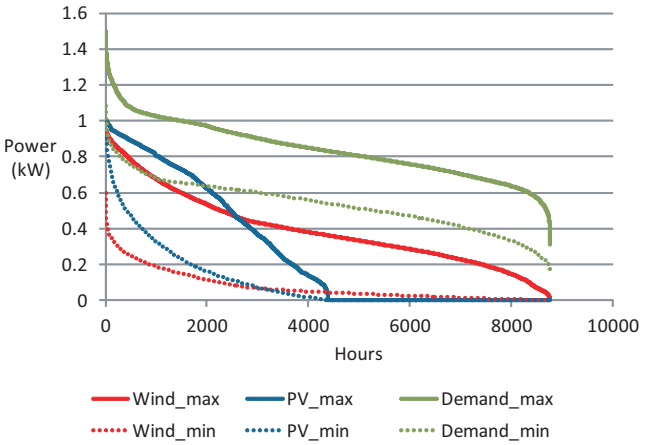

Fig. 3. Duration curves of maximum and minimum load, and wind and PV generation.

The budgets of uncertainty for each uncertain parameter range from 0 to 1 in steps of 0.1. In order to solve all the combinations, 11x11x11=1331 RMILPs were solved.

MC simulations were performed to assess which of the solutions performs best in practice. 10 scenarios were generated using the random forest algorithm [42] for each uncertain parameter, resulting in 1000 MC scenarios. Features of the three year historical data were the baseline to build the classification and regression tree used to generate MC scenarios.

VRLA and Li-Ion batteries cost 280 €/kWh and 800 €/kWh, respectively. Both charging and discharging efficiencies are set to 0.9. Batteries are considered to be 90% charged at the start of the simulation horizon and are required to end up charged beyond this level at the end of the simulation horizon. The wind turbine specific cost is 2,300 €/kW, and PV specific cost is 750 €/kW. Fuel cell specific cost is 6,300 €/kW, reservoir capacity is 100 l, reservoir replacement cost 600 €, and the hydrogen to electricity conversion ratio is taken as 660 l/kWh. The costs for batteries and distributed generation technologies are based on invoices of equipment purchased for installation at an actual telecommunications facility.

The minimum SoC threshold is set to 20%. The reasoning behind the selection of this particular value is the maximum allowable discharge conditions for different types of batteries. To that end, it is a common principle in practical applications to deploy an over-discharge protection based on the minimum voltage threshold. Once the battery reaches this value, it is strongly recommended to stop its discharge immediately because it may otherwise experience significant damage [36]. Since a detailed electrical modeling of the battery is outside the scope of this paper, and knowing that the relationship between SoC and steady state battery terminal voltage is a monotonically increasing function [36], a SoC threshold was used instead of a voltage threshold.

Motivated by industrial standards and recommendations, we assume that a reduction of battery capacity to 80% implies the end of its economic life. Due to requirements for high reliability in autonomous applications relying on batteries, this boundary has been steadily increasing over the past few

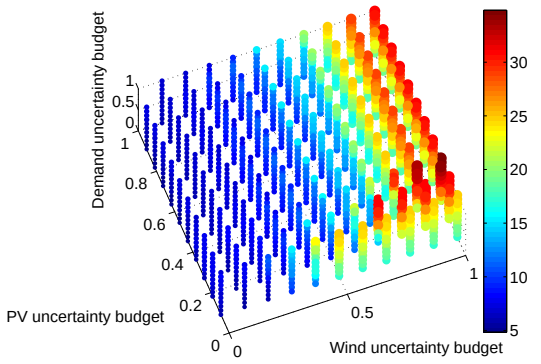

Fig. 4. Battery capacity (kWh) in case of VRLA batteries for different budgets of uncertainty.

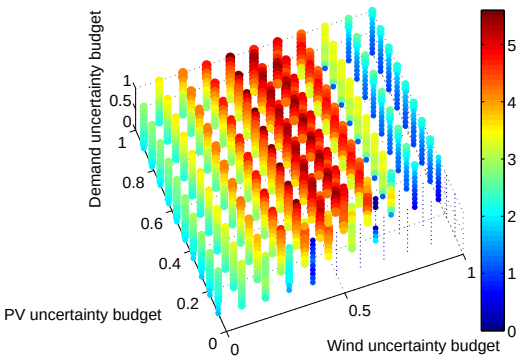

Fig. 5. Wind capacity (kW) in case of VRLA batteries for different budgets of uncertainty.

decades before finally being set at 80% [43]. The reason behind selecting this particular value is the fact that long-term cycling tests have shown that both Li-Ion and VRLA batteries start to degrade at a much faster rate once the usable capacity falls below this value [44], [45]. Nevertheless, the proposed algorithm is able to accommodate any other capacity boundary value. This will be reflected only in step 12 of the proposed solution algorithm.

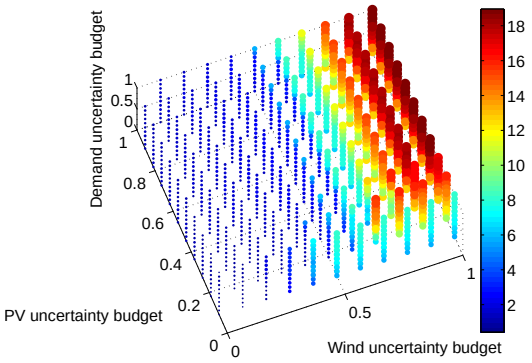

Fig. 6. PV capacity (kW) in case of VRLA batteries for different budgets of uncertainty.

B. Results

Figures 4 to 6 show the optimal battery, wind turbine and PV capacities for the VRLA batteries, while Figures 7 to 9 show in parallel the same results for Li-Ion batteries. Each of these 4-dimensional graphs shows the results for all the combinations of wind, PV and demand uncertainty budgets that were considered. The lower left corner of each chart shows less conservative results (low wind and PV uncertainty budgets), while the upper right corner shows more conservative results, corresponding to higher wind and PV uncertainty budgets. Additionally, the demand uncertainty budget grows towards the top of each column, generally resulting in higher installed capacities. The required battery, wind and PV capacities are visualized using different colors. Finally, larger capacities are represented by wider columns.

For the VRLA battery technology, the highest battery capacity is needed when the wind uncertainty is high. A wind uncertainty budget greater than 0.7 requires at least 21 kWh of battery storage, regardless of the PV and demand uncertainty. For wind uncertainty budgets lower than 0.5, the required battery capacity is not much affected by the PV's budget of uncertainty because of the low required PV capacity (left-hand side of Figure 6). If both wind and PV budgets of uncertainty are high, the model will rely more on PV generation, supported by high battery capacity (right-hand side of Figure 4). For wind uncertainty budgets lower than 0.6, almost all installed RES capacity is in the wind power (left and middle parts of Figure 5). It is only for high budgets of wind uncertainty that large amounts of PV are needed (right-hand side of Figure 6). The maximum required wind and PV capacities are 5.6 and 19 kW, respectively. Fuel cells are not used because of their high price.

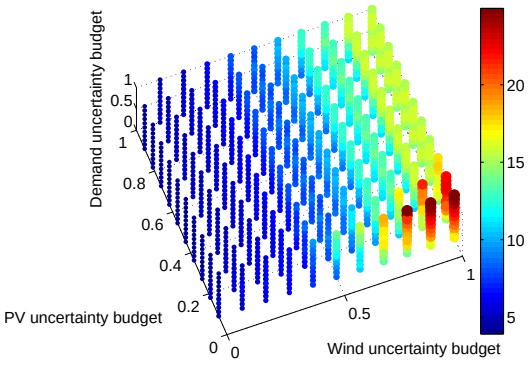

Fig. 7. Battery capacity (kWh) in case of Li-Ion batteries for different budgets of uncertainty.

Similar observations are valid for Figures 7 to 9. Since Li-Ion technology is more expensive, the optimal battery capacity in Figure 7 is lower than the one in Figure 4. This lower battery capacity is balanced by a higher wind capacity, as shown in Figure 8. The maximum required wind and PV capacities are 7.8 and 16.4 kW, respectively. As compared to the VRLA technology, the model that uses Li-Ion battery technology relies more on wind power, with the lower use of PV, as can be seen when comparing Figures 6 and 9. This indicates that PV generation requires higher battery capacities than wind generation. The required PV capacities are high only for high wind uncertainty budgets, as shown in the right-hand

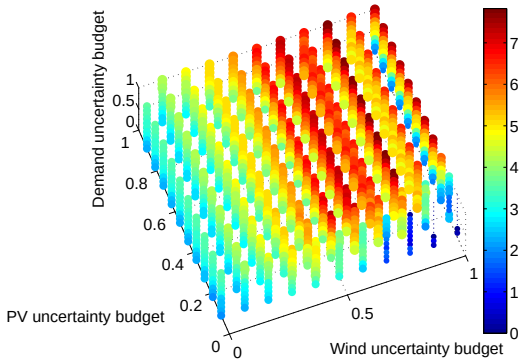

Fig. 8. Wind capacity (kW) in case of Li-Ion batteries for different budgets of uncertainty.

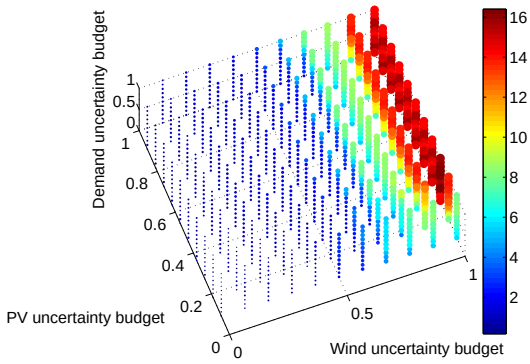

Fig. 9. PV capacity (kW) in case of Li-Ion batteries for different budgets of uncertainty.

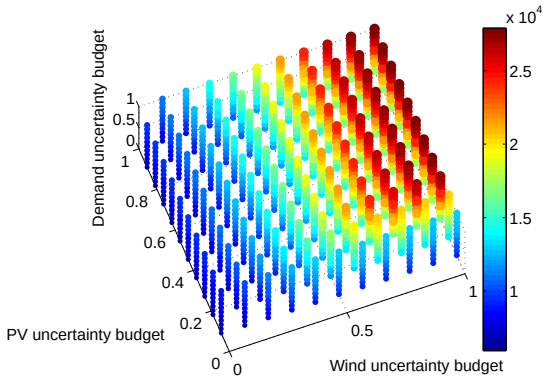

Fig. 10. Investment cost (€) in case of VRLA batteries for different budgets of uncertainty.

side of Figure 9. Fuel cells are again not used.

Figures 10 and 11 show overall investment costs for different budgets of uncertainty in case of VRLA and Li-Ion battery technology, respectively. Expectedly, investment cost increases from lower to higher uncertainty budget in all three dimensions.

Figure 12 shows the maximum number of hours with SoC below 20% over all MC generated scenarios and the average curtailed energy produced by RES as functions of the investment cost for both VRLA and Li-Ion batteries, considering total battery capacity. Clearly, the number of days where the SoC drops dangerously low decreases as the level of

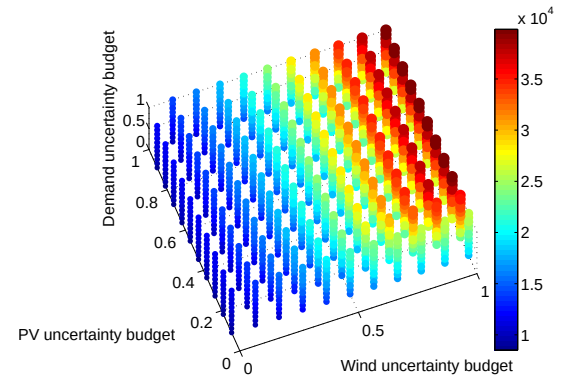

Fig. 11. Investment cost (€) in case of Li-Ion batteries for different budgets of uncertainty.

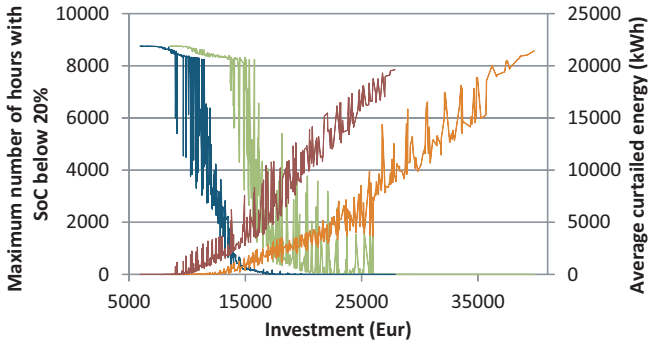

Fig. 12. Maximum number of hours with SoC below 20% in MC simulations (blue curve for VRLA, and green curve for Li-Ion technology) and average curtailed wind energy (red curve for VRLA, and orange curve for Li-Ion technology) for the initial (100%) battery capacity, all as functions of investment cost.

investment increases, while the amount of spilled renewable energy follows an opposite trend. Moreover, the valleys of blue (green) curves correspond to the peaks of red (orange) curves and vice versa. In order for a solution to be feasible, the maximum number of hours at the with SoC below 20% over all test scenarios has to be 0, which yields the minimum investment of 18,196 € for VRLA batteries and 27,505 € for Li-Ion batteries. Table I provides a more detailed analysis of these solutions.

For VRLA batteries the optimal solution is obtained for the following uncertainty budgets: $\Gamma_{\mathrm{d}} = 0.1$, $\Gamma_{\mathrm{pv}} = 0.2$ and $\Gamma_{\mathrm{w}} = 0.8$. The optimal generation mix consists of 18.04 kWh of VRLA battery capacity, 9.49 kW of PV capacity and 2.62 kW

TABLE I
RESULT COMPARISON

	VRLA	Li-Ion
$\Gamma_{\mathrm{d}}/\Gamma_{\mathrm{pv}}/\Gamma_{\mathrm{w}}$	0.1/0.2/0.8	0.4/0.1/0.8
ESS capacity	18.04 kWh	14.65 kWh
PV capacity	9.49 kW	6.51 kW
Wind turbine capacity	2.62 kW	4.74 kW
Investment cost	18,196 €	27,505 €
Annual wind curtailment	9,178 kWh	8,652 kWh
Annual battery capacity reduction	5.5%	1.2%

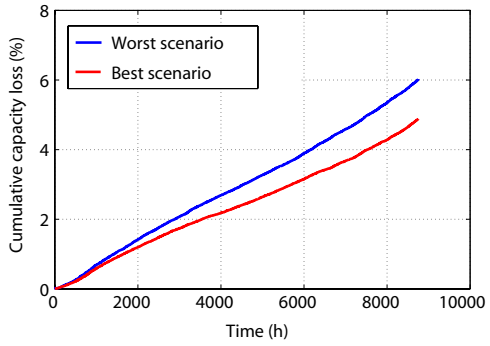

Fig. 13. Annual cumulative loss of VRLA battery capacity.

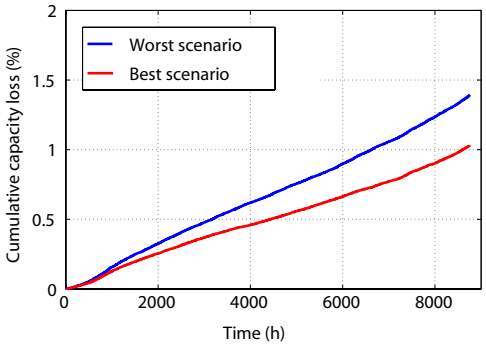

Fig. 14. Annual cumulative loss of Li-Ion battery capacity.

of wind turbine capacity. The investment cost is 18,196 € and average annual RES curtailment is 9,178 kWh. Applying the cycle counting algorithm to all MC scenarios, the annual loss of capacity ranges from 4.88% up to 6.07%. The cumulative capacity loss for these two extreme scenarios is plotted in Figure 13. Based on the average of all scenarios, the expected battery capacity reduction is 5.5% per year. This means that the usable battery capacity will drop to 80% in 3.9 years, when the battery stack will need to be replaced. This adds additional cost of 1,295 €/year.

For the Li-Ion technology, the optimal mix consists of 14.65 kWh of Li-Ion battery capacity, 6.51 kW of PV capacity and 4.74 kW of wind turbine capacity. This solution was obtained for the following uncertainty budgets: $\Gamma_{\mathrm{d}} = 0.4$, $\Gamma_{\mathrm{pv}} = 0.1$ and $\Gamma_{\mathrm{w}} = 0.8$. Due to the higher cost of this technology, the battery capacity is 19% lower than for VRLA. PV capacity is reduced by 31%. This is compensated by an increase in wind turbine capacity of 81%. The investment cost is 27,505 € and the average annual RES curtailment is 8,652 kWh. The expected annual battery capacity reduction was calculated using the same method as for the VRLA technology. Figure 14 shows minimum and maximum battery capacity loss scenarios. An average loss of capacity of 1.2% per year indicates that the batteries will need to be replaced in 18.5 years. This yields an additional annual cost of 634 €/year. Although the cost of Li-Ion batteries is much higher than VRLA batteries, significantly lower battery degradation yields much lower additional annual cost. The overall cost, depending on the facility lifetime, is shown in Figure 15. If the telecommunication facility's lifetime is longer than 14 years, Li-Ion battery technology is cheaper than VRLA technology.

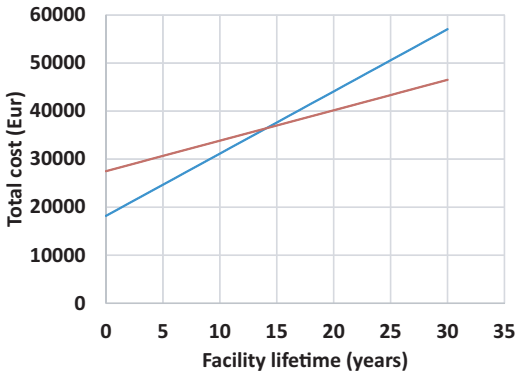

Fig. 15. Overall cost of supplying the telecommunications facility depending on its lifetime.

C. Influence of Cycling

The SoC analysis in Figure 12 assumes the initial battery capacity throughout the year. However, this capacity is monotonously decreasing as the batteries cycle. Figure 16 shows the maximum number of hours with SoC below 20% over all MC scenarios and the average curtailed energy produced by RES as functions of the investment cost, but in the case of usable battery capacity of 80%, simulating battery operation towards the end of their lifetime. The graphs in this figure are almost identical to the ones in Figure 12, which indicates that the reduction in battery capacity due to degradation does not significantly decrease their expected minimum SoC during operation. Figure 17 shows the maximum number of hours with SoC below 20% in MC simulations for a usable battery capacity of 80% for solutions that had zero days with SoC below 20% for the initial case. In other words, Figure 17 shows the increase in forbidden SoC for investments that were not forbidden in Figure 12. The optimal solution for VRLA battery technology now has at most 12 hours with a minimum SoC below 20% (the first point of the red graph), while the optimal solution for the Li-Ion battery technology now has at most 4 hours with the minimum SoC below 20% (the first point of the blue graph). Since batteries are considered to be towards the end of their lifetime, this violation should be tolerated. Moreover because the investment cost would be 19,775 € for the VRLA technology (an increase of 8.7%), and 32,641 € for the Li-Ion technology (an increase of 18.7%) if one would want to keep SoC above 20% even towards the end of battery lifetime.

D. Computational Issues

The RMILP was solved using CPLEX 12.1 under the GAMS 23.7 environment on an Intel i7 1.8 GHz processor with 4 GB of memory. Depending on the uncertainty budget, each RMILP computation required from 1 to 4 min. Since the RMILP was solved 1331 times, it took almost 2 days to obtain the results for each battery technology.

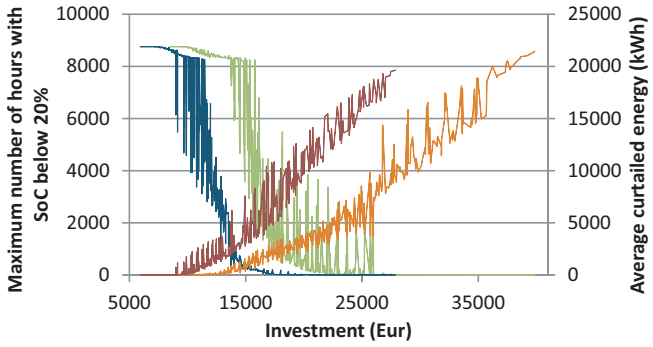

Fig. 16. Maximum number of hours with SoC below 20% in MC simulations (blue curve for VRLA, and green curve for Li-Ion technology) and average curtailed wind energy (red curve for VRLA, and orange curve for Li-Ion technology) for 80% usable battery capacity, all as functions of investment cost.

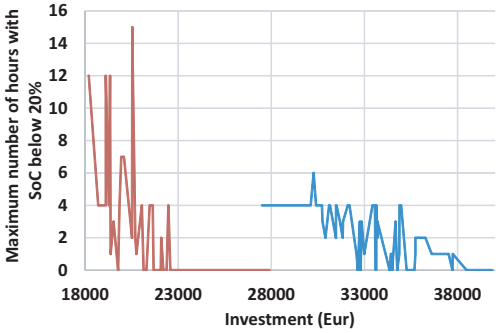

Fig. 17. Maximum number of hours with SoC below 20% in MC simulations for usable battery capacity of 80% for solutions with zero days with SoC below 20% for the initial case.

Running RMILP solutions against a set of scenarios is not an issue since the first time a SoC below a given limit, e.g. 20%, is detected, that solution is immediately discarded. For the purpose of this paper, a complete set of 1.3 million scenario checks was run in both Microsoft Excel and Matlab, which lasted for 26 hours in Matlab and 3 days in Microsoft Excel.

Since the battery capacity reduction is calculated only for the most promising solutions, its computational burden is negligible.

VI. Conclusion

This paper has presented a procedure for minimizing investments in supplying an autonomous remote facility based on RMILP. The advantage of this technique is its flexibility in terms of solution accuracy and computational burden, both being controlled by the number of uncertainty budgets used. The model identifies the optimal RES and ESS mix based on the telecommunications facility lifetime, as the attractiveness of various battery technologies depends on it.

The results of the case study indicate that when facility lifetime is longer than 14 years, the high cost of frequent replacements of VRLA batteries might result in a higher total cost than when Li-Ion batteries are used. Although Li-Ion batteries have a higher investment cost, infrequent replacements make this technology more attractive. Additionally, as shown in Figure 17, the SoC of Li-Ion batteries suffer less violation towards the end of the battery lifetime.

ESS and RES capacities were considered to be continuous variables in this case study. In real-world applications, with predetermined manufacturer for each type of equipment, these variables might be integers. However, this would have a negative effect to the computational time.

Solving this problem requires a significant amount of computing resources. However, this should not be an issue since this type of simulation is performed off-line only once in the design stage of the project.

The off-line computation of the influence of battery degradation surely results in a suboptimal solution. Future research should therefore aim to incorporate the cycle counting algorithm actively rather than treating it as endogenous.

References

[1] C. Hernandez-Aramburo, T. Green, and N. Mugniot, "Fuel consumption minimization of a microgrid," *IEEE Trans. Ind. Appl.*, vol. 41, no. 3, pp. 673–681, 2005.

[2] K. Sun, L. Zhang, Y. Xing, and J. Guerrero, "A distributed control strategy based on dc bus signaling for modular photovoltaic generation systems with battery energy storage," *IEEE Trans. Power Electron.*, vol. 26, no. 10, pp. 3032–3045, 2011.

[3] T. Hirose and H. Matsuo, "Standalone hybrid wind-solar power generation system applying dump power control without dump load," *IEEE Trans. Ind. Electron.*, vol. 59, no. 2, pp. 988–997, 2012.

[4] F. Blaabjerg, R. Teodorescu, M. Liserre, and A. Timbus, "Overview of control and grid synchronization for distributed power generation systems," *IEEE Trans. Ind. Electron.*, vol. 53, no. 5, pp. 1398–1409, 2006.

[5] J. Peas Lopes, C. Moreira, and A. Madureira, "Defining control strategies for microgrids islanded operation," *IEEE Trans. Power Syst.*, vol. 21, pp. 916–924, May 2006.

[6] N. Hatziargyriou, H. Asano, R. Iravani, and C. Marnay, "Microgrids," *Power and Energy Mag., IEEE*, vol. 5, pp. 78–94, July 2007.

[7] H. Kakigano, Y. Miura, and T. Ise, "Low-voltage bipolar-type dc microgrid for super high quality distribution," *IEEE Trans. Power Electron.*, vol. 25, pp. 3066–3075, Dec 2010.

[8] J. Guerrero, J. Vasquez, J. Matas, L. de Vicuna, and M. Castilla, "Hierarchical control of droop-controlled ac and dc microgrids - a general approach toward standardization," *IEEE Trans. Ind. Electron.*, vol. 58, no. 1, pp. 158–172, 2011.

[9] N. Pogaku, M. Prodanovic, and T. Green, "Modeling, analysis and testing of autonomous operation of an inverter-based microgrid," *IEEE Trans. Power Electron.*, vol. 22, pp. 613–625, March 2007.

[10] F. Katiraei and M. Iravani, "Power management strategies for a microgrid with multiple distributed generation units," *IEEE Trans. Power Syst.*, vol. 21, pp. 1821–1831, Nov 2006.

[11] R. Majumder, B. Chaudhuri, A. Ghosh, R. Majumder, G. Ledwich, and F. Zare, "Improvement of stability and load sharing in an autonomous microgrid using supplementary droop control loop," *IEEE Trans. Power Syst.*, vol. 25, pp. 796–808, May 2010.

[12] T.-L. Lee, S.-H. Hu, and Y.-H. Chan, "D-statcom with positive-sequence admittance and negative-sequence conductance to mitigate voltage fluctuations in high-level penetration of distributed-generation systems," *IEEE Trans. Ind. Electron.*, vol. 60, pp. 1417–1428, April 2013.

[13] X. Wang, F. Blaabjerg, and Z. Chen, "Autonomous control of inverter-interfaced distributed generation units for harmonic current filtering and resonance damping in an islanded microgrid," *IEEE Trans. Ind. Appl.*, vol. 50, pp. 452–461, Jan 2014.

[14] Q.-C. Zhong, "Robust droop controller for accurate proportional load sharing among inverters operated in parallel," *IEEE Trans. Ind. Electron.*, vol. 60, pp. 1281–1290, April 2013.

[15] Q. Shafiee, C. Stefanovic, T. Dragicevic, P. Popovski, J. Vasquez, and J. Guerrero, "Robust networked control scheme for distributed secondary control of islanded microgrids," 2013.

[16] S. Sucic, J. G. Havelka, and T. Dragicevic, "A device-level service-oriented middleware platform for self-manageable dc microgrid applications utilizing semantic-enabled distributed energy resources," *Int. Journal of Elec. Power En. Sys.*, vol. 54, no. 0, pp. 576 – 588, 2014.

[17] T. Dragicevic, J. Guerrero, J. Vasquez, and D. Skrlec, "Supervisory control of an adaptive-droop regulated dc microgrid with battery management capability," *IEEE Trans. Power Electron.*, vol. 29, no. 2, pp. 695–706, 2014.
[18] "Microgrid deployment tracker 2q13n." http://www.reportlinker.com/p01187963-summary/Microgrid-Deployment-Tracker-2Q13.html. Accessed: 2014-03-19.
[19] W. Zhou, C. Lou, Z. Li, L. Lu, and H. Yang, "Current status of research on optimum sizing of stand-alone hybrid solar-wind power generation systems," *Appl. Energy*, vol. 87, no. 2, pp. 380 – 389, 2010.
[20] P. Brown, J. Peas Lopes, and M. Matos, "Optimization of pumped storage capacity in an isolated power system with large renewable penetration," *IEEE Trans. Power Syst.*, vol. 23, no. 2, pp. 523–531, 2008.
[21] C. Abbey and G. Joos, "A stochastic optimization approach to rating of energy storage systems in wind-diesel isolated grids," *IEEE Trans. Power Syst.*, vol. 24, no. 1, pp. 418–426, 2009.
[22] Y. Atwa and E. El-Saadany, "Optimal allocation of ess in distribution systems with a high penetration of wind energy," *IEEE Trans. Power Syst.*, vol. 25, no. 4, pp. 1815–1822, 2010.
[23] L. Xu, X. Ruan, C. Mao, B. Zhang, and Y. Luo, "An improved optimal sizing method for wind-solar-battery hybrid power system," *IEEE Trans. Sustain. Energy*, vol. 4, no. 3, pp. 774–785, 2013.
[24] Y. Katsigiannis, P. Georgilakis, and E. Karapidakis, "Hybrid simulated annealing - tabu search method for optimal sizing of autonomous power systems with renewables," *IEEE Trans. Sustain. Energy*, vol. 3, no. 3, pp. 330–338, 2012.
[25] A. Bansal, R. Kumar, and R. Gupta, "Economic analysis and power management of a small autonomous hybrid power system (sahps) using biogeography based optimization (bbo) algorithm," *IEEE Trans. Smart Grid*, vol. 4, no. 1, pp. 638–648, 2013.
[26] J. C. Spall, *Introduction to Stochastic Search and Optimization: Estimation, Simulation, and Control*. Wiley, 2003.
[27] D. Bertsimas, E. Litvinov, X. Sun, J. Zhao, and T. Zheng, "Adaptive robust optimization for the security constrained unit commitment problem," *IEEE Trans. Power Syst.*, vol. 28, no. 1, pp. 52–63, 2013.
[28] D. Bertsimas and M. Sim, "The price of robustness," *Operations Research*, vol. 52, no. 1, pp. pp. 35–53, 2004.
[29] B. Borowy and Z. Salameh, "Methodology for optimally sizing the combination of a battery bank and pv array in a wind/pv hybrid system," *IEEE Trans. Energy Conv.*, vol. 11, no. 2, pp. 367–375, 1996.
[30] H. Bindner, T. Cronin, P. Lundsager, and R. D. W. E. D. Risø National Lab., *Lifetime Modelling of Lead Acid Batteries*. Contract ENK6-CT-2001-80576, 2005.
[31] V. Agarwal, K. Uthaichana, R. DeCarlo, and L. Tsoukalas, "Development and validation of a battery model useful for discharging and charging power control and lifetime estimation," *IEEE Trans. Energy Conv.*, vol. 25, no. 3, pp. 821–835, 2010.
[32] A. Bryant, P. Mawby, P. Palmer, E. Santi, and J. Hudgins, "Exploration of power device reliability using compact device models and fast electrothermal simulation," *IEEE Trans. Ind. Appl.*, vol. 44, no. 3, pp. 894–903, 2008.
[33] M. Musallam and C. Johnson, "Real-time compact thermal models for health management of power electronics," *IEEE Trans. Power Electron.*, vol. 25, no. 6, pp. 1416–1425, 2010.
[34] L. Baringo and A. Conejo, "Offering strategy via robust optimization," *IEEE Trans. Power Syst.*, vol. 26, no. 3, pp. 1418–1425, 2011.
[35] D. Bertsimas, E. Litvinov, X. Sun, J. Zhao, and T. Zheng, "Adaptive robust optimization for the security constrained unit commitment problem," *IEEE Trans. Power Syst.*, vol. 28, no. 1, pp. 52–63, 2013.
[36] D. Linden and T. B. Reddy, *Handbook of Batteries*. McGraw-Hill, 2002.
[37] L. H. Thaller, "Expected cycle life versus depth of discharge relationships of well behaved single cells and cell strings," in *162nd Meeting of the Electrochem. Soc., Detroit, 17-22 Oct. 1982* (M. S. Baxa and C. E. Weinlein, eds.), pp. 17–22, 1982.
[38] D. Vutetakis and H. Wu, "The effect of charge rate and depth of discharge on the cycle life of sealed lead-acid aircraft batteries," in *IEEE 35th International Power Sources Symposium*, pp. 103–105, 1992.
[39] B. Cotton, "Vrla battery lifetime fingerprints - part 1," in *IEEE 34th International Telecommunications Energy Conference (INTELEC)*, pp. 1–8, 2012.
[40] M. Swierczynski, *Lithium ion battery energy storage system for augmented wind power plants*. PhD Thesis, 2012.
[41] M. Musallam and C. Johnson, "An efficient implementation of the rainflow counting algorithm for life consumption estimation," *IEEE Trans. Reliab.*, vol. 61, no. 4, pp. 978–986, 2012.
[42] L. Breiman, "Random forests," *Mach. Learn.*, vol. 45, no. 1, pp. 5–32, 2001.
[43] W. Reeve, *DC Power System Design for Telecommunications*. IEEE Telecommunications Handbook Series, Wiley, 2006.
[44] "Ieee recommended practice for maintenance, testing, and replacement of vented lead-acid batteries for stationary applications," *IEEE Std 450-2010 (Revision of IEEE Std 450-2002)*, pp. 1–71, Feb 2011.
[45] M. Swierczynski, D. Stroe, A.-I. Stan, R. Teodorescu, and D. Sauer, "Selection and performance-degradation modeling of limo ˙2 /li ˙4 ti ˙5 o ˙12 and lifepo ˙4 /c battery cells as suitable energy storage systems for grid integration with wind power plants: An example for the primary frequency regulation service," *IEEE Trans. Sust. En.*, vol. 5, pp. 90–101, Jan 2014.

Tomislav Dragičević (S'09−M'13) received the M.E.E. and the Ph.D. degrees from the Faculty of Electrical Engineering, Zagreb, Croatia, in 2009 and 2013, respectively. Since 2010, he has been actively cooperating in an industrial project related with design of electrical power supply for remote telecommunication stations. He is currently a full-time Postdoc at Aalborg University in Denmark. His research interests include modeling, control and energy management of flexible microgrids.

Hrvoje Pandžić (S'06−M'12) received the M.E.E and Ph.D. degrees from the Faculty of Electrical Engineering, University of Zagreb, in 2007 and 2011, respectively. He is currently a postdoctoral researcher at the University of Washington, Seattle, WA, USA. His research interests include planning, operations, control and economics of power and energy systems.

Davor Škrlec (M'90) received the M.S. and the Ph.D. degrees in electrical engineering from the University of Zagreb, Faculty of Electrical Engineering and Computing, in 1990 and 1996, respectively. He is a Full Professor of the Department of Energy and Power Systems, Faculty of Electrical Engineering and Computing, University of Zagreb, His research and professional interests include planning and operation of electrical power networks, distributed energy resources, power systems economics, and geographic information system applications in the power utilities. He has published more than 50 papers from his area of interest and he is author and coauthor of several professional books. He is a Principal Investigator and Project Leader of several projects funded by industry and government. Core activities within the research activities are focused on optimal planning and operation of active distribution networks and microgrids. Dr. Škrlec is an active member of CIGRE and CIRED.

Igor Kuzle (S'94−M'97−SM'04) is an Associate Professor at the University of Zagreb Faculty of Electrical Engineering, Department of Energy and Power Systems. He was the project leader for more than 50 technical projects for industry and electric power companies. His scientific interests include problems in electric power systems dynamics and control, unit commitment, maintenance of electrical equipment, as well as power system analysis and integration of renewable energy sources. Prof. Kuzle has been the IEEE PES Chapter Representative for Central Europe and Scandinavia in IEEE Region 8 since 2010.

Josep M. Guerrero (S'01−M'04−SM'08) received the B.S. degree in telecommunications engineering, the M.S. degree in electronics engineering, and the Ph.D. degree in power electronics from the Technical University of Catalonia, Barcelona, in 1997, 2000, and 2003, respectively. He was an Associate Professor with the Department of Automatic Control Systems and Computer Engineering, Technical University of Catalonia, teaching courses on digital signal processing, field programmable gate arrays, microprocessors, and control of renewable energy. Since 2011, he has been a Full Professor with the Department of Energy Technology, Aalborg University, Aalborg, Denmark, where he is responsible for the microgrid research program. Since 2012, he has also been a Guest Professor at the Chinese Academy of Science and the Nanjing University of Aeronautics and Astronautics.

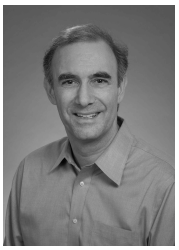

Daniel S. Kirschen (M'86−SM'91−F'07) received the electrical and mechanical engineer's degrees from the Universit Libre de Bruxelles, Belgium, in 1979, and the M.S. and Ph.D. degrees from the University of Wisconsin, Madison, in 1980 and 1985, respectively. He is currently Close Professor of Electrical Engineering at the University of Washington, Seattle.